J Mater Sci (2007) 42:923–934
DOI 10.1007/s10853-006-0011-1

MWCNT reinforced Polyamide-6,6 films: preparation, characterization and properties

Rajatendu Sengupta · Anirban Ganguly · S. Sabharwal · Tapan K. Chaki · Anil K. Bhowmick

Received: 5 November 2005 / Accepted: 14 March 2006 / Published online: 2 January 2007

Abstract Composite films of Polyamide-6,6 (PA66) and multi-walled carbon nanotubes (MWCNTs) were prepared by a combination of solution casting followed by compression molding techniques. Both unfunctionalized (u-MWCNTs) and functionalized nanotubes (f-MWCNTs) were used in this study. The functionalization involved direct solvent-free amination of MWCNTs with hexamethylenediamine. Thermogravimetric analysis was used to observe the changes in the nanotubes upon functionalization and morphological features of the resulting composite films were studied using scanning electron microscopy, transmission electron microscopy, and atomic force microscopy. The crystallinity changes by incorporation of the u-MWCNTs and f-MWCNTs in the PA66 matrix were studied by wide angle X-ray scattering and differential scanning calorimetry. The f-MWCNT/PA66 film showed an improvement of ~43% in maximum tensile stress (MTS) and ~32% in Young's modulus over pristine PA66 film, while at a similar loading of 0.5 wt%, the f-MWCNT/PA66 film showed ~15% increase in MTS and ~16% increase in modulus over the u-MWCNT/PA66 film. Dynamic mechanical analysis indicated significant difference in the small-strain mechanical properties between the MWCNT-filled and unfilled PA66 at the very low MWNT loadings that were tested and supported the tensile results. The water absorption trend of the composite films showed dramatic improvement over the neat film.

R. Sengupta · A. Ganguly · T. K. Chaki · A. K. Bhowmick (✉)
Rubber Technology Centre, Indian Institute of Technology, Kharagpur 721302, India
e-mail: anilkb@rtc.iitkgp.ernet.in

S. Sabharwal
Radiation Technology Development Section, BARC, Trombay, Mumbai 400085, India

Introduction

Carbon nanotubes (CNTs) classified as a one-dimensional carbon system because of their high aspect ratio [1] are being extensively studied since their discovery by Iijima [2], due to their unique mechanical, electrical, thermal and other properties [1, 3, 4]. However, the most important application of CNTs, based on their mechanical properties is as a reinforcement agent in polymer composites. Moreover, due to the very high aspect ratio of CNTs, the electrical conductivity of these composites shows the percolation behavior at relatively low CNT contents [5]. Although CNT-filled polymer composites are the obvious choice of researchers after the success with carbon-fiber reinforced polymer composites, the effective utilization of CNTs depends upon three factors: homogeneous dispersion of CNTs in the polymer matrix while maintaining the integrity of the tubes, alignment of the nanotubes and formation of strong interfaces between the CNT and polymer matrix [6, 7]. Researchers have reported the use of both single-walled carbon nanotubes (SWCNTs) and multi-walled carbon nanotubes (MWCNTs) with and without functionalization to reinforce polymer matrices [8–18]. Previous researchers have functionalized CNTs in order to promote interfacial interactions between the nanotubes and polymeric matrices leading to better reinforcement. In this article, we report the results based on both

unfunctionalized and amine-functionalized MWCNTs. Till now the methods of fabrication of the CNT-based composites include the sonication of pure or functionalized nanotubes in a polymer solution [11, 12], in situ polymerization in the presence of CNTs [19], melt mixing [16–18] and melt processing after solution mixing [9]. This article reports the characteristics of MWCNT reinforced poly (iminohexamethyleneiminoadipoyl) (better known as Polyamide-6,6) films prepared by the sonication of MWCNTs in polymer solution followed by casting and subsequent compression molding. To the best of our knowledge, no previous work involving CNTs in PA66 exists and a comparative study of the u-MWCNT and f-MWCNT reinforced PA66 films in terms of morphological, thermal, mechanical, dynamic mechanical, and water absorption results is reported for the first time.

Nanocomposites from other types of fillers, namely silica and clay have been reported extensively in the literature [20, 21]. For example, nanoclay reinforced polymers have been shown to impart improved tensile behavior, ductility, and barrier properties at a very low loading of the filler. Similarly, the silica/polymer hybrids display new properties for optical, electrical, structural, and related applications [20]. We have also reported from our laboratory, preparation and properties of various nanoclay/rubber and nanosilica/polymer composites [22, 23]. PA66/silica hybrid nanocomposites have also been developed in our laboratory [24] and this work extends our efforts in this field.

Experimental

Preparation of MWCNT/PA66 composite films

A commercial grade of PA66 (Zytel 101L, DuPont, India) was dissolved in 100% formic acid (GR) of Merck Ltd., India to prepare a 10 wt% PA66 solution. MWCNT (CVD MWNT 95) from Iljin Nanotech Co., Korea having a carbon content of about 95% was used as received. The MWCNTs were grown by the chemical vapor deposition (CVD) process and the diameter and length of the nanotubes were ~10–20 nm and ~10–50 μm, respectively (Fig. 1). Hexamethylenediamine (HMDA) (synthesis grade) of Merck Schuchardt, Germany was used for amination of the nanotubes and ethanol (synthesis grade) of Merck Ltd., India was used as the solvent for HMDA.

The MWCNTs were functionalized following the procedure outlined by Basiuk et al [25]. In brief, 100 mg of MWCNT and 2 g of HMDA were taken in a thick-walled Borosil test tube (50 ml capacity) and heated in an oil-bath to 393–403 K for 12 h. During the course of the reaction, HMDA melted and the nanotubes remained immersed in the HMDA melt. Some HMDA also evaporated and condensed at the top end (cooler part) of the test tube. The amine-functionalized nanotubes (f-MWCNTs) were transferred while hot from the test tube to a beaker and were freed of the excess amine by washing with ethanol ten times (10 min sonication) and successive filtration through a sintered disc crucible by application of slight vacuum. The filtered f-MWCNTs were further washed with distilled water, filtered and then dried in a vacuum oven, characterized and subsequently used for the composite preparation. The duration of the functionalization was varied and after each functionalization and purification procedure (to free the f-MWCNTs from the excess amine), the f-MWCNTs were subjected to FT-IR and TGA studies. It was observed that exposing the MWCNTs to a time greater than 12 h (we exposed the MWCNTs to the amination reaction up to 36 h) did not cause any further change in the FT-IR or TGA results. Thus, the functionalization of the MWCNTs was optimized.

For the preparation of the MWCNT reinforced composites, the requisite amount of MWCNT (functionalized or unfunctionalized) was initially sonicated (Elma GmbH, 40 W) in formic acid for 1 h and was then added to the 10% PA66 solution and the resulting mixture was mechanically stirred for 1 h at 300–400 rpm. Then the dispersion was sonicated for 1 h and finally again mechanically stirred for 1 h at 300–400 rpm to prepare the MWCNT/PA66 dispersion. It is known that ultrasonic treatment of the nanotubes

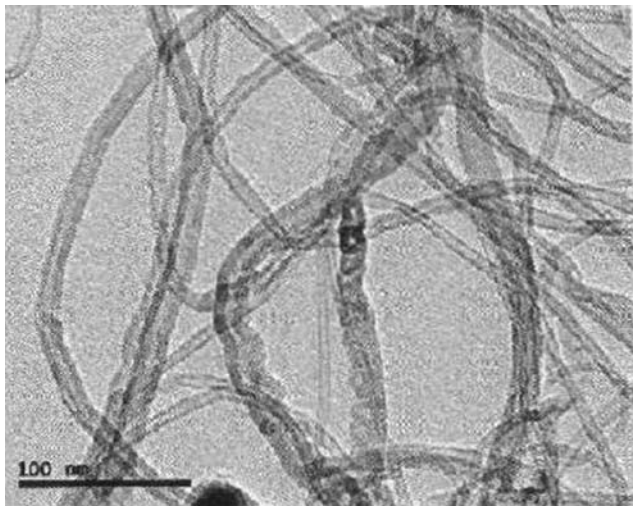

Fig. 1 TEM micrograph of as-supplied MWCNT (TEM image courtesy of Iljin Nanotech Co., Korea)

results in damage by introduction of defects into the MWCNTs [26] and so the sequence of operations was optimized for the composition containing 0.5 wt% of u-MWCNTs and was subsequently applied to the other compositions. The dispersions were finally poured on thoroughly cleaned glass plates for room temperature (298 K) drying in a fume hood to constant weight. The air-dried films on the glass plates were opaque and extremely adherent and thus had to be scrapped with a stainless steel spatula for removal. The resultant films were vacuum dried for 24 h at 353 K and subsequently compression molded in between Teflon sheets at 553 K for 6 min for obtaining self-standing films. A minimum of three films were prepared and from each film, a minimum of two tensile specimens were die-punched. The thicknesses of the films were 100 ± 10 μm for all the samples. The u-MWCNT content in the polymer matrix was varied from 0.5 to 2.0 wt% on the basis of 100 g of PA66. The f-MWCNT loading in PA66 was studied at two concentrations, viz. 0.5 and 1.0 wt% on the basis of 100 g of PA66. The 1.0 wt% f-MWCNT/PA66 composite sample was prepared to observe the tensile behavior when the addition of f-MWCNT was increased slightly. The films were stored in a desiccator to minimize moisture ingress. However, during synthesis and testing of the hybrid composite films, the relative humidity in air was ~80%. All the films were prepared at the same time and thus were subjected equally to the ambient conditions of temperature and humidity. Pure PA66 films were prepared similarly. The designations of the compression-molded films are tabulated in Table 1.

Characterization of the nanotubes and the prepared films

Fourier transform infrared (FT-IR) spectroscopic analyses of the nanotubes were carried out under ambient conditions using a Perkin-Elmer FT-IR spectrometer Spectrum RX I at a resolution of 4 cm^{-1}. The nanotubes (2 mg) were mixed with KBr (198 mg) and pressed into a thin circular disc for the FT-IR study. Thermogravimetric analysis (TGA) of the nanotubes was conducted using TGA Q 50 of TA Instruments-Waters LLC, USA at a heating rate of 10 K min^{-1} in the temperature range of 313–1073 K under oxygen flow rate of 60 ml min^{-1}.

Table 1 Designation of the compression molded films

Sample designation	PA66 (%)	MWCNT (%)	Comments
NC0	100	–	Neat PA66 film
NC05	100	0.5	0.5 wt% u-MWCNT loaded film
NC1	100	1.0	1.0 wt% u-MWCNT loaded film
NC2	100	2.0	2.0 wt% u-MWCNT loaded film
NC05m	100	0.5	0.5 wt% f-MWCNT loaded film
NC1m	100	1.0	1.0 wt% f-MWCNT loaded film

The dispersion of the MWCNTs in the PA66 matrix was visually compared using digital images taken with a Dimage Z1 digital camera (Minolta, Japan). Scanning electron microscopy (SEM) was performed using a JEOL JSM 5800 scanning electron microscope. For SEM, the fractured cross-section of thicker films (~300 μm) after tensile failure was photographed. The films were coated with gold by sputtering. For transmission electron microscopy (TEM) measurements, 100 nm sections were microtomed at 213 K using Ultracut E ultramicrotome by Reichert and Jung using a diamond knife. Measurements were carried out with a Tecnai G^2 TEM (120 kV) and the digital images were acquired using a Gatan Model 791 side mount camera.

Tapping mode atomic force microscopy (AFM) images of the CNT loaded films were taken with Nanoscope IIIa of Veeco-Digital Instruments with tapping mode etched silicon probes (RTESP) having a resonance frequency of ~280 kHz and spring constant ~40 N/m. Typical scan rate for image acquisition was ~1.0 line/s. The images were obtained under ambient laboratory conditions and no filtering or other image processing operations were performed to generate the images.

Wide angle X-ray scattering (WAXS) data were collected in digital form from the films using a Philips 1710 X-Ray diffractometer operated at 40 kV and 20 mA with Cu Kα radiation source. The scan rate was 3°min^{-1}. WAXS data were collected on films, which were annealed at 473 K for 3 h. The area under the crystalline and amorphous portions was determined in arbitrary units and the percent crystallinity was calculated using the following equation:

$$\%\,\text{crystallinity} = \frac{I_C}{I_C + I_A} \times 100 \quad (1)$$

where I_C and I_A are the integrated intensities corresponding to the crystalline and amorphous phases, respectively. The crystallinity values reported are the average values based on three experiments per sample. The scans were profile fitted by using standard software (ORIGIN 7.0).

Differential scanning calorimetry (DSC) measurements of the pure PA66 and the MWCNT/PA66 films were performed using a DSC model Q 100 of TA Instruments-Waters LLC, USA with nitrogen as the purge gas. The machine was calibrated according to the elaborate procedure mentioned in the DSC manual using indium and sapphire at a heating rate of 10 K min^{-1} and the maximum error in temperature as a result was within ±0.5 K. In the heating scan, the films were heated from 303 to 573 K at a heating rate of 10 K min^{-1}. The films were held for 5 min at 573 K to eliminate the previous heat history completely before cooling to 303 K at 10 K min^{-1}. The second heating run was started after equilibration of the cooled films at 303 K and a similar protocol was followed as the first heating run. For determining the crystallinity from the DSC heating runs, the heat of fusion of a 100% crystalline PA66 was taken to be 190 kJ/kg [27] and the following equation was used:

$$\%\,\text{crystallinity} = \frac{\Delta H_{EXP}}{\Delta H_F} \times 100 \quad (2)$$

where ΔH_{EXP} is the actual heat of fusion of the sample under study and ΔH_F is the heat of fusion of 100% crystalline PA66. DSC was conducted on films which were annealed at 473 K for 3 h.

Measurement of film properties

Measurement of mechanical properties of the composites was carried out using a Zwick 1445 Universal Testing Machine at a cross-head speed of 50 mm min^{-1}. The tensile specimens were punched from the compression molded films using ASTM Type IV die. The tests were carried out as per ASTM D 638-98 at 298 ± 2 K. The average value of five tests was used for reporting and the samples tested were in the Dry-As-Molded (DAM) state.

Dynamic mechanical analysis (DMA) of the films were performed using DMA 2980 Dynamic Mechanical Analyzer of TA Instruments-Waters LLC, USA in tension film mode in the temperature range of 303–473 K at a frequency of 1 Hz and heating rate of 2 K min^{-1}. The storage modulus (E') and loss tangent (tan δ) were measured as a function of temperature for all the DAM specimens.

Water absorption tendency of neat PA66 and the MWCNT reinforced PA66 films were evaluated by immersing equal weights of the sample films in water for 120 h at ambient temperature (298 K). The water uptake was calculated using the following formula:

$$\%\,\text{water uptake} = \frac{\text{final weight} - \text{initial weight}}{\text{initial weight}} \times 100 \quad (3)$$

Results and discussion

Characterization of MWCNTs

The FT-IR traces of u-MWCNTs and f-MWCNTs are compared in Fig. 2. The FT-IR spectra are of poor quality primarily due to the absorption by the MWCNTs and also due to the low concentration of the organic moieties attached to the nanotubes. However, the characteristic N–H stretch in the 3500–3300 cm^{-1} region and N–H deformation in the ~1600 cm^{-1} region is more prominent in the f-MWCNT spectrum compared to the u-MWCNT spectrum. This was also previously reported by Basiuk et al. [25] for 1-octadecylamine modified MWCNT.

The thermogravimetric analysis (TGA) of the MWCNTs reveals that the u-MWCNTs start losing weight from 760 K, whereas the f-MWCNTs do so gradually from 473 K (Fig. 3a). The loss of weight for the u-MWCNTs is in line with the reported value of 740 K for pristine MWCNTs at a heating rate of 10 K min^{-1} in air by Zou et al [28]. The derivative thermogravimetric (DTG) peak degradation temperatures of u-MWCNT and f-MWCNT are at 889 and 879 K (Fig. 3b) and these indicate that the shift in the

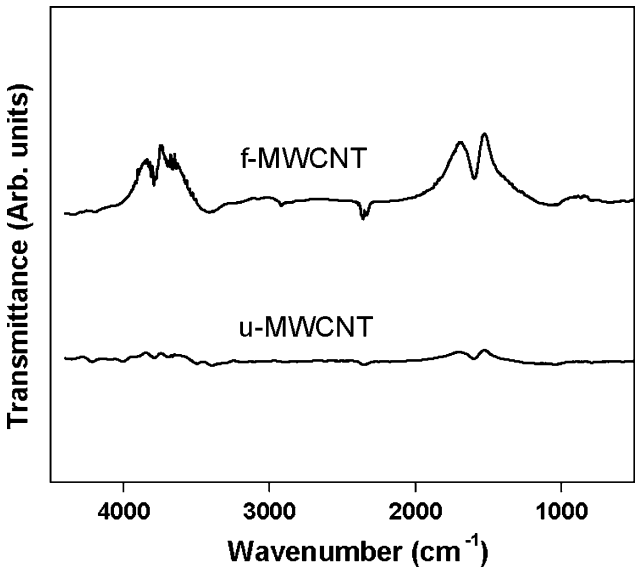

Fig. 2 FT-IR spectra of u-MWCNT and f-MWCNT

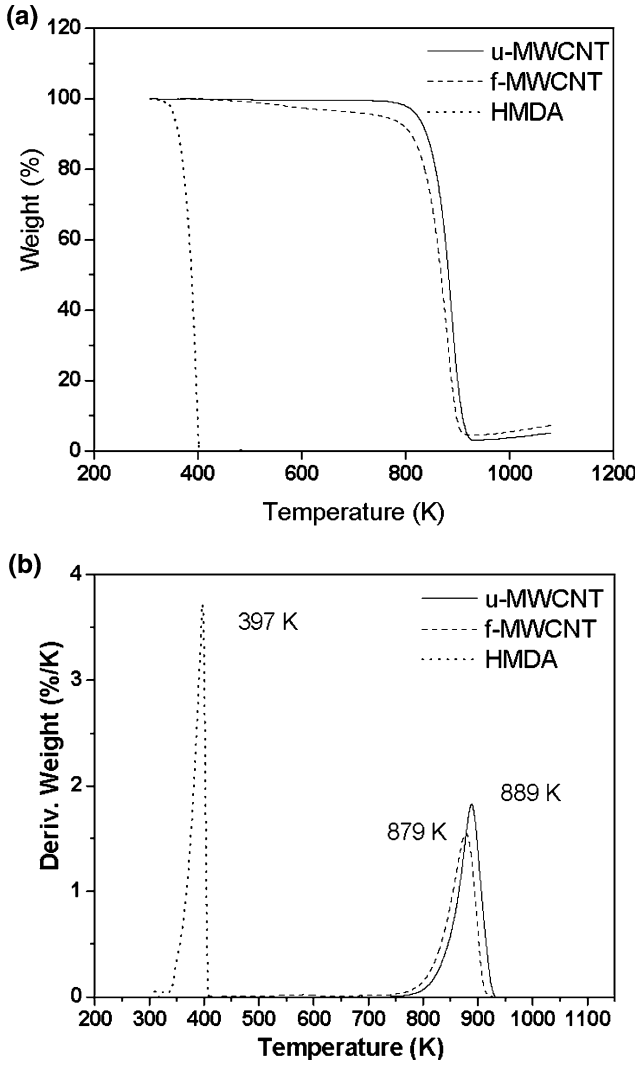

Fig. 3 (**a**) TGA curves of u-MWCNT, f-MWCNT, and HMDA, (**b**) DTG curves of u-MWCNT, f-MWCNT, and HMDA

maximum decomposition temperature is due to the functionalization of the nanotubes. The TGA of HMDA is also shown along with the nanotubes in Fig. 3a, b. The DTG peak of HMDA occurs at ~397 K and it is observed that HMDA remaining is less than 1.0 wt% at 480 K. The HMDA molecules are not just simply physisorbed on the sidewalls of the nanotubes since physisorbed HMDA molecules would get removed at temperatures lower than 673 K and thus are chemically attached to the sidewalls and the defect sites on the nanotubes. Similar conclusions were drawn by Basiuk et al. [25] with their 1-octadecylamine derivatized MWCNTs.

Characterization of the films

The digital photographs shown in Fig. 4a–d compare the overall distribution of the MWCNTs on the

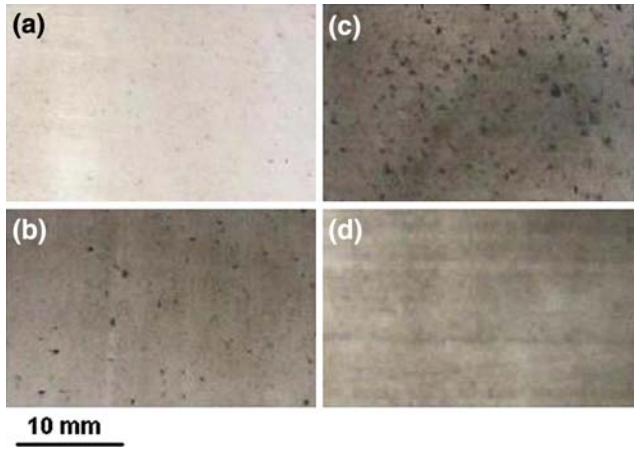

Fig. 4 Digital photographs of (**a**) NC05, (**b**) NC1, (**c**) NC2, and (**d**) NC05m. Agglomerates are more evident in (**b**) and (**c**). All photographs have the same magnification

millimeter scale for NC05, NC1, NC2, and NC05m, respectively. It is evident that on the millimeter scale the distribution of the unfunctionalized nanotubes is not uniform even after melt mixing and that the number of u-MWCNT agglomerates increases with nanotube loading. These observations are similar to those obtained by Haggenmueller et al. [9] for SWCNT–PMMA nanocomposites and by Bhattacharyya et al. [29] for melt-blended PP/SWCNT composites. However, the f-MWCNTs are homogeneously dispersed in the polymer matrix and therefore the appearance of the NC05m film is grayish compared to NC05 film.

Figure 5a shows the SEM image of NC05 after tensile failure. The nanotubes are seen to be randomly oriented in the matrix. It is easily observed that there is a significant bridging action of the u-MWCNT between the polymer fracture surfaces. Like in conventional fiber composites, nanotube pull-out and fracture is also noticeable in Fig. 5a. Figure 5b provides an enlarged view of a bridging u-MWCNT between the polymer surfaces. This bridging action would result in increased tensile strengths as reported below. The length of the exposed MWCNT is ~6 μm. Its thickness varies from 140 to 190 nm in contrast to the dimensions given in Fig. 1 and this may be due to the bundling up of a few nanotubes and also due to the matrix encapsulating the nanotube. Further, the sputtered gold coating used to make the samples conductive for using in our SEM needs to be taken into account when measuring the thickness for the bridging nanotube. However, some of the scattered nanotubes in Fig. 5a have the dimensions lower than 90 nm. Figure 5c shows the SEM image of the NC05m composite film in the fractured area after the tensile test. The nanotubes (some of the nanotubes

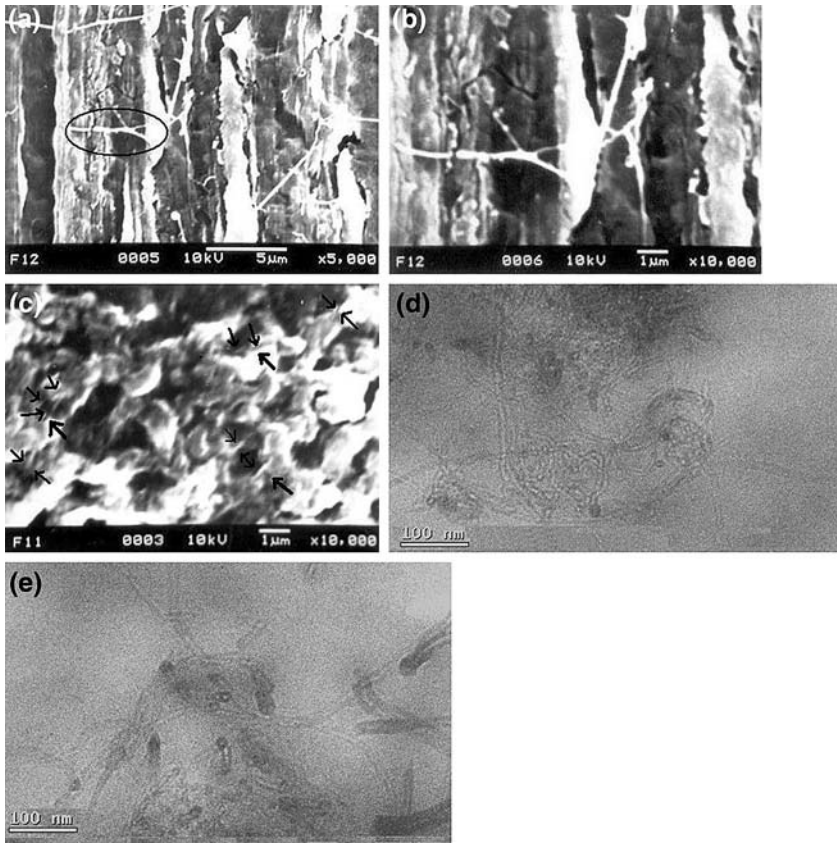

Fig. 5 SEM micrograph of NC05 after tensile test in (**a**) and zoom up of an individual nanotube in (**b**). The portion enlarged is marked in (**a**) by an ellipse. (**c**) SEM micrograph of NC05m after tensile test. (**d**) TEM image of NC05. (**e**) TEM image of NC05m

are marked by arrows for visual detection) are seen to be uniformly scattered throughout the matrix. The exposed (pull-out) portions of the amine-functionalized nanotubes are also covered with the polymeric matrix in Fig. 5c. In this case, the nanotubes are not completely pulled out from the matrix (while nearly complete pull-out of the nanotube is noticed in Fig. 5b) implying greater anchoring and/or interactions as a result of functionalization. Due to the presence of amine functional groups, the anchoring/interacting sites between the f-MWCNT and the polymer matrix increase, and these increased interactions between the f-MWCNT and the PA66 matrix are responsible for the increased tensile properties of NC05m over those of NC05 as mentioned later. Moreover, this favorable interaction (polar–polar interactions between the amine groups and the polar –CONH– groups along the PA66 chain) results in increased compatibility between the f-MWCNTs and the matrix leading to better dispersion due to a lowering of the interfacial tension. The average dimensions of the exposed f-MWCNTs vary from 50 to 80 nm and this is ascribed to the better dispersion than the u-MWCNTs. Representative TEM images of NC05 and NC05m are shown in Fig. 5d and e, respectively. It is evident that the dispersion of the f-MWCNTs is better than that of the u-MWCNTs and bundling is more for the u-MWCNTs compared to f-MWCNTs. The curvy nature of both types of nanotubes is evident from the TEM images. However, the darkening of the f-MWCNT sidewalls and tube ends indicate amorphous material originating from the HMDA molecules bound to the defect sites [25].

Representative AFM photographs of the composite films are shown in Fig. 6a–c. AFM phase images of NC05 and NC05m are shown in Fig. 6a and b, respectively. The nanotubes in Fig. 6a appear to have diameter of 20–40 nm (the values were obtained quantitatively by AFM section analysis) and this increase is due to the matrix covering the nanotubes. The spaghetti-like structure of u-MWCNTs is clearly perceptible in the bottom portion of Fig. 6a. Evidently, some parts of the nanotube are above the film surface and some parts are embedded within the PA66 matrix. Some nanotube ends (which are perpendicular to the plane of the image) are also noticeable in the same figure. The AFM phase image of NC05m shown in Fig. 6b shows very uniform distribution of the nanotubes in the matrix. The section analysis of the amine-modified nanotubes exhibits the diameter ranging from 20 to 30 nm. Section analysis of nanotube-agglomerated region in

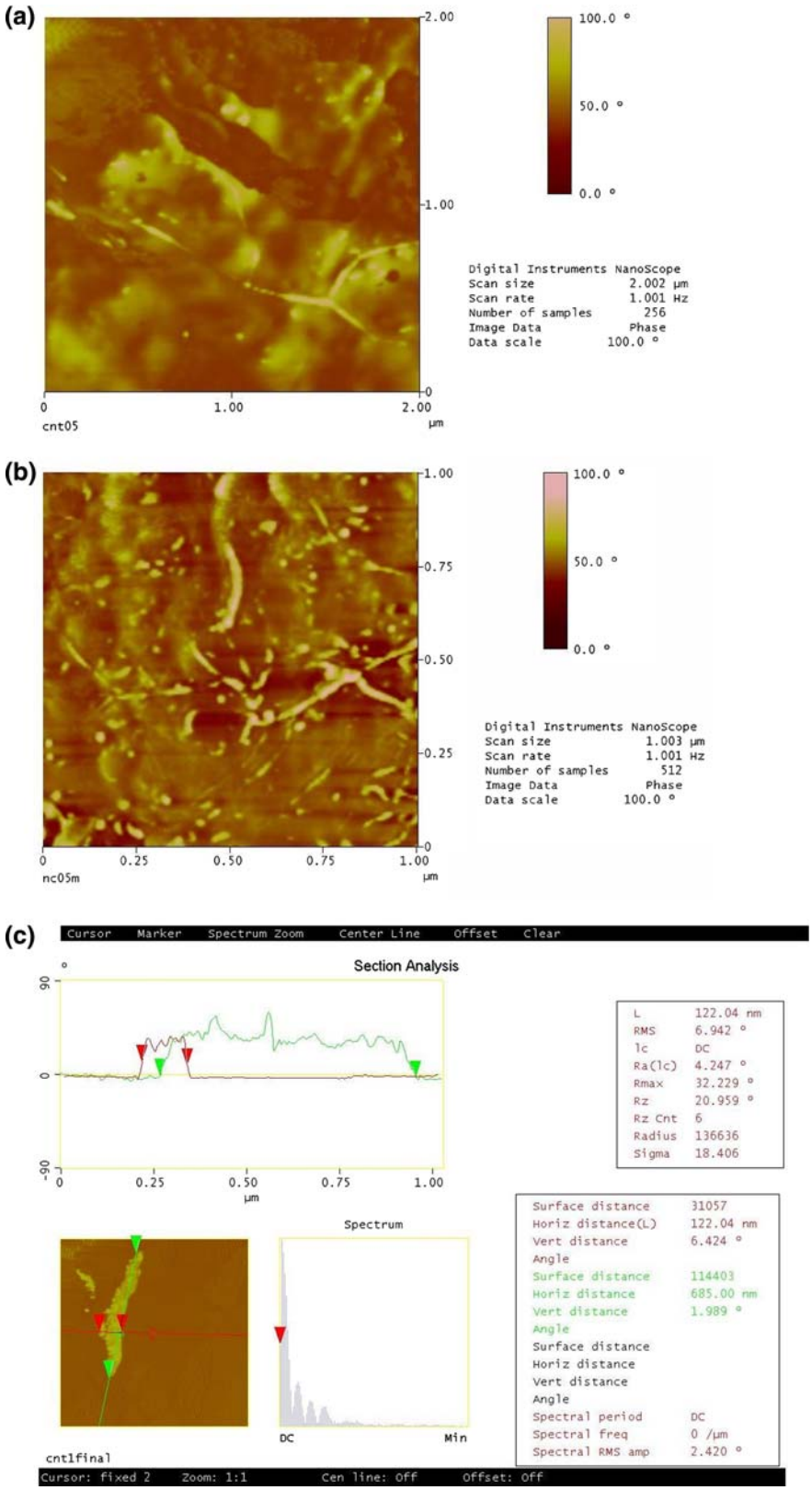

Fig. 6 (**a**) AFM phase image of NC05. (**b**) AFM phase image of NC05m. (**c**) AFM section analysis of NC1

NC1 (Fig. 6c) gives the horizontal length (L) as 122 nm and this implies that several nanotubes are bundled up within the matrix.

Dispersion and orientation of the nanotubes does influence the mechanical performance and hence, the dispersions were checked over a large number of

samples. Both the TEM and AFM images do not reveal any preferred orientation of the nanotubes and functionalization does not change the picture. The only aspect affected is that the dispersion probably gets better with functionalization of the nanotubes and this gets reflected in the tensile and dynamic mechanical properties.

WAXS was used to investigate the changes in crystalline structure of the MWCNT/PA66 films. Usually, the appearance of peaks at 2θ values of ~20.2° and 23.6° signifies the existence of the α-phase in PA66. It has been reported that PA66 exists in the α- and β-crystalline forms at room temperature [30]. However, PA66/clay nanocomposites under certain circumstances give rise to the γ crystalline phase (consisting of the γ1 and γ2 peaks) along with the α phase (consisting of α1 and α2 peaks) at room temperature [31]. The WAXS scans of the annealed films stacked in Fig. 7 show the presence of the α1, α2, γ1, and γ2 peaks at ~20.3°, 23.6°, 13.6°, and 22.0°, respectively. The α1 peak arises from the distance between the hydrogen-bonded chains while the α2 peak arises from the separation of the hydrogen-bonded sheets. The α1 peak intensity is more than that of α2 peak in all the films. The variation in the peak positions for the films—NC0, NC05, NC1, NC2, and NC05m are negligible (within ±0.1 and hence within experimental error) and hence not reported here. However, the presence of the γ1 and γ2 peaks in all the samples proves that it is an artifact of the solution casting and/or the thermal history and not due to the presence of MWCNT in the PA66 matrix. The presence of the (002) peak intensity at ~26° (2θ) due to the MWCNTs [32] is almost non-existent due to the low level of CNT loading and does not seem to affect the WAXS profiles of PA66.

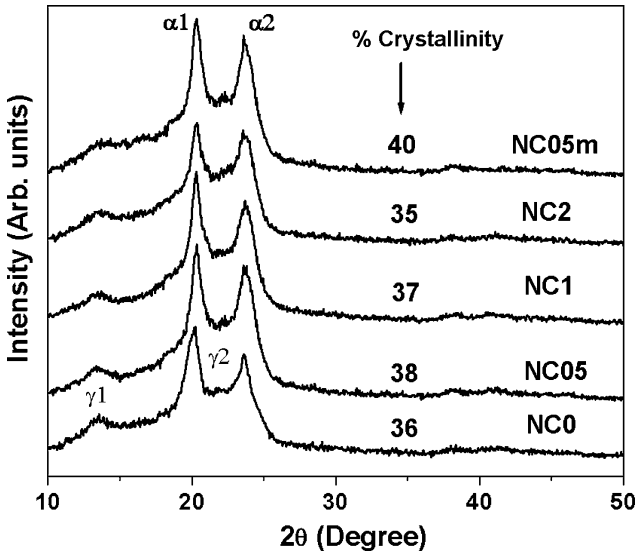

Fig. 7 WAXS profiles of the annealed films. The curves are vertically offset for clarity

The relative crystallinity values from the WAXS scans are mentioned in Fig. 7 against the corresponding curves. NC05m, which contains f-MWCNTs, shows the highest crystallinity content of 40% among all the films. It is further observed that the crystallinity increases from 36% to 38% in the films NC0 and NC05 and then again decreases from 37% to 35% in the films NC1 and NC2. Further support for the WAXS results come from the DSC scans.

The DSC first heat provides useful information about the polymer crystallization that has occurred due to the thermo-mechanical processing of the polymer. Figure 8a shows the first heating DSC traces of the films where the change in the enthalpy values (ΔH_{EXP}) and the variation of melt temperature (T_m) can be noted with MWCNT loading. Since the films were annealed, the DSC first heating traces help in understanding the role of MWCNTs in inducing crystallinity changes in the PA66 matrix. Among all the films, NC05m shows the highest ΔH_{EXP} value and thus the highest crystallinity. The crystallinity values of NC0, NC05, NC1, NC2, and NC05m calculated using Eq. 2 (the ΔH_{EXP} values were corrected by linear weighted averaging of the PA66 and MWCNT weight contributions) were 41%, 47%, 43%, 37%, and 51% respectively. This trend mirrors the crystallinity trend from the WAXS studies. However, the melt temperatures (T_m) show no significant difference.

The DSC second heating scans of the polymer films are shown in Fig. 8b and evaluate the effect of MWCNTs on the films which have been subjected to an equivalent thermal history. Here also, the film containing 0.5 wt% f-MWCNT loading exhibits the highest enthalpy value of 84 kJ/kg. The percent crystallinity calculated for NC0, NC05, NC1, NC2, and NC05m are 35%, 42%, 36%, 35%, and 44%, respectively. Therefore, at equivalent thermal histories, the 0.5 wt% f-MWCNT loaded film exhibits more crystallinity than the u-MWCNT loaded films. As observed in the first heating runs, the variation in T_m remains marginal also in the second heating runs.

The crystallization exotherms of the films are compared in Fig. 8c. The onset (T_{onset}) and peak (T_p) temperatures and heat of crystallization (ΔH_C) of the films are mentioned against the curves in Fig. 8c. It is observed that the crystallization temperature (T_p) increases marginally with the introduction of the nanotubes indicating that nanotubes nucleate crystallization. Functionalization of the nanotubes leads to a

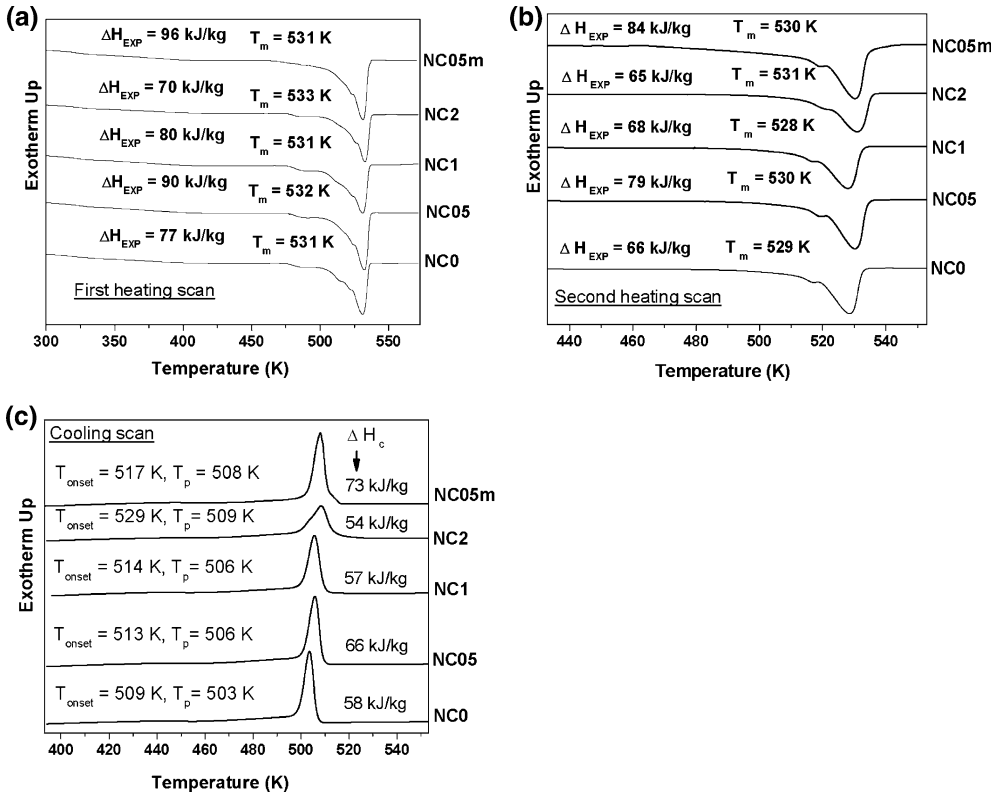

Fig. 8 (**a**) DSC curves obtained from the first heating scan for the films. (**b**) DSC curves obtained from the second heating scan for the films. (**c**) Non-isothermal crystallization thermograms of the films at a cooling rate of 10 K mn^{-1}

far greater extent of nucleation than the unfunctionalized nanotubes (at equivalent nanotube loading, i.e., at 0.5 wt% loading). Most probably, better dispersion of the f-MWCNTs leads to generation of more accessible heterogeneous nucleation sites and thus NC05m film has the higher heat of crystallization than the NC05 film. Further, the onset temperature has also increased for all the nanotube loaded films compared to neat PA66 indicating that the composite films start crystallization at higher temperature than the neat PA66 film (i.e., NC0) does. However, even though the u-MWCNTs induce nucleation in PA66, the very high aspect ratios and most probably interfacial interactions between MWCNTs and the amide groups situated along the PA66 chains result in confinement and restriction of the movement of the PA66 molecules leading to lower crystallization rates in the PA66/MWCNT composite films. This restriction in the movement of the PA66 molecules probably increases with the concentration of u-MWCNT and this ultimately leads to a lowering of the overall crystallinity in the NC1 and NC2 composite films after the initial crystallinity increase in NC05 composite film. Similar interfacial interactions between MWCNT and EVA (ethylene-*co*-vinyl acetate copolymer) leading to lower crystallization rates have been reported by Li et al. [33].

Typical stress–strain curves for the DAM films are presented in Fig. 9a and maximum tensile stress, Young's modulus and elongation at break (EB) behavior for all the films are compared in Fig. 9b. The tensile property values for neat PA66 shown in Fig. 9b are considerably lower than that for injection-molded bulk specimen data of the manufacturer (the DAM yield stress and Young's modulus values of neat Zytel 101L are 83 and 3,100 MPa, respectively) [34]. This is probably due to sample preparation by compression molding technique and the molding conditions [24]. All the MWCNT/PA66 composite films show an increase in Young's modulus over neat PA66 film. CNT acts as the hard phase in the soft polymeric phase and so addition of CNT would result in the increase of modulus of the composite. The modulus value of NC05m is highest among all the films studied (~32% increase over NC0 and ~16% increase over NC05) and this can be ascribed to maximum crystallinity and best dispersion among all the nanotube-reinforced films. It is well known that in semicrystalline polymers like PA66, the crystallinity plays a major role in shaping the mechanical properties. Further, the increased interactions between amine groups on the f-MWCNT surface and the PA66 as mentioned previously leads to better interfacial adhesion favoring stress transfer from the matrix to the f-MWCNTs. Among the u-MWCNT

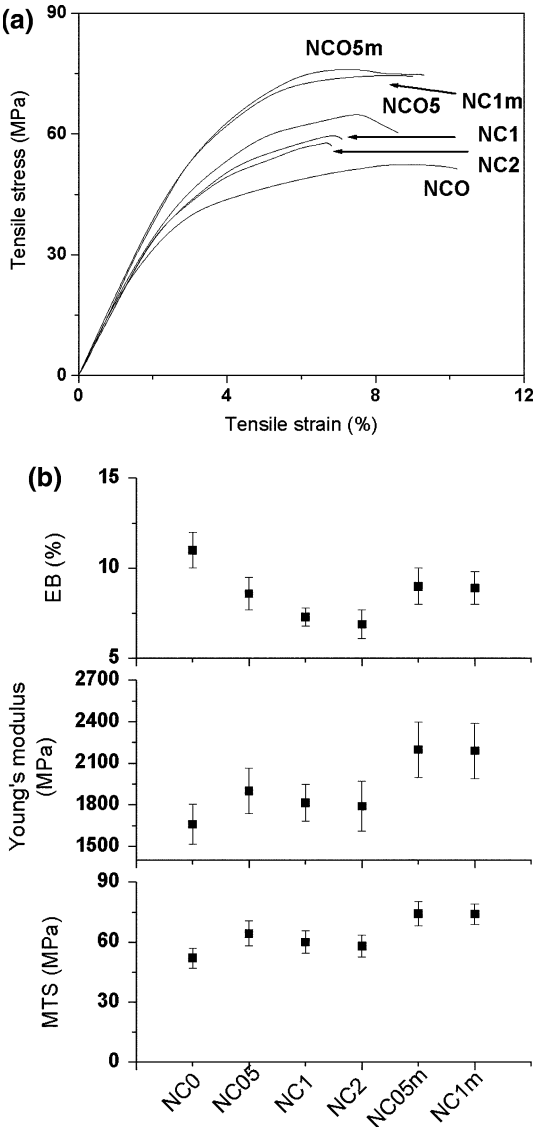

Fig. 9 (**a**) Typical engineering tensile stress-strain curves for the as-prepared DAM films. (Those curves which had their maximum tensile stress values closer to the mean maximum tensile stress values were chosen as the representative stress-strain curves.) (**b**) Comparison of maximum tensile stress (MTS), Young's modulus and elongation at break (EB) for the as-prepared DAM films

reinforced composite films, the Young's modulus value reaches a maximum for the NC05 film and then drops gradually to lower values for the higher CNT loadings of 1 and 2 wt%. With a very small loading of 0.5 wt% u-MWCNT, the crystallinity has been shown to increase as already mentioned in the discussion under WAXS and DSC results. This increase in crystallinity in NC05 leads to an increased modulus value over NC0, NC1, and NC2. The increase in modulus for the NC05 film over NC0 is ~14% while the improvements are ~ 9% and 8%, respectively for NC1 and NC2 over NC0. It is well known that for effective reinforcement, good nanotube dispersion is necessary.

The effect of functionalization is also evident in the maximum tensile stress (MTS) trend. The increase in MTS of NC05m is ~43% while that of NC05 is ~24% over NC0. In spite of the not so excellent nanotube dispersion in the films having u-MWCNT loadings of 1 and 2 wt%, the modulus and MTS values are more than that of neat PA66 film. Both modulus and MTS should have increased with increasing CNT loading but due to poor dispersion the values are lower than those obtained with CNT loading of 0.5 wt%. Also, the crystallinity decreases with nanotube loading after 0.5 wt%. Bhattacharya et al. [29] reported no improvement in the tensile properties of SWCNT loaded polypropylene composite and they had attributed this to the presence of large nanotube aggregates due to poor dispersion of the SWCNT in the polymer matrix. In the present work, all the MWCNT loaded films exhibited lower EB values than the neat film and this means that the composites become brittle with increasing nanotube loading. The data for NC1m suggests that the tensile properties of the functionalized MWCNT loaded PA66 films plateau out at 1 wt% f-MWCNT loading.

The variation of tan δ and storage modulus (E') with temperature for the films are shown in Fig. 10a and b, respectively. The glass transition temperature (T_g) of NC0 occurs at ~349 K and for NC05, NC1, NC2 and NC05m the T_g does not vary much. So the presence of nanotubes in the matrix does not affect the tan δ peak position. However, the tan δ peak heights of NC05 and NC05m are significantly lower than that of NC0 (inset of Fig. 10a). The peak height of NC05m is lower than that of NC05. In semicrystalline polymers like PA66, a decrease in tan δ peak height implies an increase in crystallinity [35] and evidence for the crystallinity increase comes from the WAXS and DSC studies. It is seen that the storage modulus (E') values for all the nanotube loaded films are above that of the neat film in the temperature range of 298–473 K and can be explained on the basis of both crystallinity and reinforcing action of nanotube loading. Among all the films, NC05m exhibits the highest E' value and this may be reasoned on the basis of increased crystallinity resulting from the good dispersion of the nanotubes in the matrix due to functionalization of the nanotubes. The storage modulus value of NC05 is next to that of NC05m and this is due to the lower crystallinity as a result of dispersion of unfunctionalized nanotubes. The E' value of NC1 is higher than that of NC2 and this may be due to better dispersion of nanotubes in the former as evidenced from Fig. 4. The remarkable

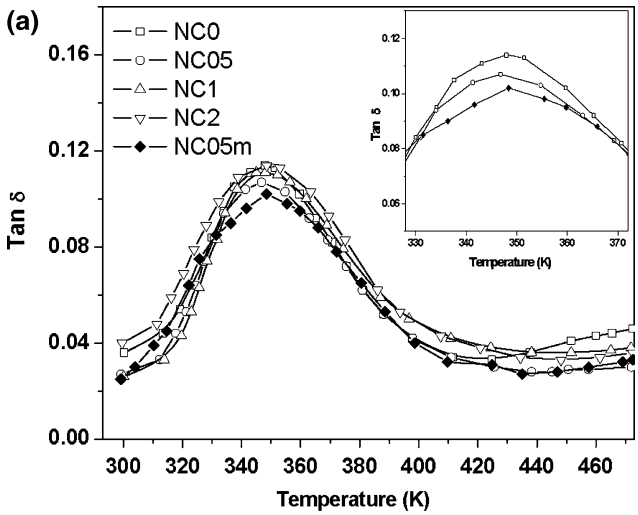

Fig. 10 (**a**) Tan δ curves for the DAM films. Inset compares the height of NC0, NC05, and NC05m. (**b**) Storage modulus (E') curves of the DAM films

feature of all the nanotube loaded films are that the E' values are significantly higher than the neat PA66 film even at higher temperatures. Schaffer et al. [8] reported a similar improvement of E' values at higher temperatures in CNT reinforced poly (vinyl alcohol) composite films. At T_g, the E' values for NC05m, NC05, NC1, and NC2 are greater than the E' value of NC0 by ~62%, 51%, 35%, and 27%, respectively, and at 453 K, the corresponding increases are ~182%, 141%, 114%, and 87%, respectively. Thus the small-strain mechanical responses of the polymer with and without nanotubes corroborate the trend in the large-strain findings from the tensile tests.

The water uptake characteristics of unannealed films are compared in Fig. 11. It is observed that the water absorbing tendency progressively decreases by ~3.0%, 6.5%, and 10.0% with increasing u-MWCNT loading.

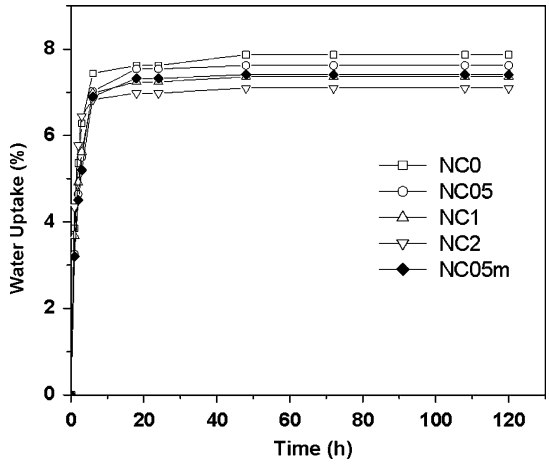

Fig. 11 Water uptake characteristics of the unannealed films

NC05m exhibits ~6% lower water uptake than NC0 and this is ~3.0% lower than the water uptake of NC05. Lower water absorption is a key property improvement especially for polyamides like PA66. The nanotubes probably impede the penetration of the water molecules and this leads to decreased water absorption. With functionalization, the nanotubes are better dispersed in the PA66 matrix and hence NC05m shows increased resistance to water absorption than NC05.

Conclusions

MWCNTs were functionalized by direct amination with HMDA. The unfunctionalized and functionalized MWCNT/PA66 composite films were prepared by solution casting followed by compression molding. SEM, TEM, and AFM reveal that the 0.5 wt% f-MWCNTs are more homogeneously distributed than 0.5 wt% u-MWCNTs in the PA66 matrix. AFM studies revealed that the CNT dispersion deteriorated with increasing unfunctionalized CNT loading. Functionalization of the nanotubes leads to increase in percent crystallinity as evidenced from both WAXS and DSC studies. With a very low loading of 0.5 wt% u-MWCNT in PA66, the maximum tensile stress and Young's modulus improved over the neat PA66 film by ~24% and 14%, respectively. Further CNT loading does not improve these tensile properties over NC05 and this is explained on the basis of dispersion problem of the CNTs in the PA66 matrix and also due to the crystallization behavior of the MWCNTs. However, PA66 loaded with 0.5 wt% f-MWCNT exhibited ~15% improvement in maximum tensile stress and ~16% improvement in modulus over NC05. The presence of the nanotubes increases the stiffness of the composite

particularly at higher temperatures as reflected from the storage modulus values. Water absorption decreases remarkably with increasing nanotube concentration and more so at equivalent loading for the functionalized nanotubes over the unfunctionalized ones. This work probably paves the path for preparing stronger lightweight PA66-based nanocomposites suitable for use as advanced composites.

Acknowledgement We acknowledge the financial assistance provided by DAE, BRNS, Mumbai (sanction no. 2002/35/7/BRNS/172).

References

1. Ajayan PM, Zhou OZ (2001) In: Dresselhaus MS, Dresselhaus G, Avouris P (eds) Carbon nanotubes: synthesis, structure, properties and applications. Topics in applied physics. Springer-Verlag, Heidelberg, p 391
2. Iijima S (1991) Nature 354:56
3. Ajayan PM (1999) Chem Rev 99:1787
4. Thostenson ET, Ren Z, Chou T-W. (2001) Compos Sci Technol 61:1899
5. Potschke P, Bhattacharya AR, Janke A (2004) Eur Polym J 137:137
6. Salvetat JP, Briggs GAD, Bonard J-M, Bacsa RR, Kulik AJ, Stockli T, Burnham NA, Forro L (1999) Phys Rev Lett 82:944
7. Ajayan PM, Schaedler LS, Giannaris C, Rubio A (2000) Adv Mater 12:750
8. Shaffer MSP, Windle AH (1999) Adv Mater 11:937
9. Haggenmueller R, Gommans HH, Rinzler AG, Fischer JE, Winey KI (2000) Chem Phys Lett 330:219
10. Jin Z, Pramoda KP, Xu G, Goh SH (2001) Chem Phys Lett 337:43
11. Qian D, Dickey EC, Andrews R, Rantell T (2002) App Phys Lett 76:2868
12. Star A, Stoddart JF (2002) Macromolecules 35:7516
13. Mitchell CA, Bahr JL, Arepalli S, Tour JM, Krishnamoorti R (2002) Macromolecules 35:8825
14. Hill DE, Lin Y, Rao AM, Allard LF, Sun Y-P (2002) Macromolecules 35:9466
15. Velasco-Santos C, Martinez-Hernandez AL, Fisher FT, Ruoff R, Castano VM (2003) Chem Mater 15:4470
16. Zhang WD, Shen L, Phang IY, Liu T (2004) Macromolecules 37:256
17. Meincke O, Kaempfer D, Weickmann H, Friedrich C, Vathauer M, Warth H (2004) Polymer 45:739
18. Bhattacharyya AR, Potschke P, Abdel-Goad M, Fischer D (2004) Chem Phys Lett 392:28
19. Kumar S, Dang TD, Arnold FE, Bhattacharyya AR, Min BG, Zhang X, Vaia RA, Park C, Adams WW, Hauge RH, Smalley RE, Ramesh S, Willis PA (2002) Macromolecules 35:9039
20. Wen J, Wilkes GL (1996) Chem Mater 8:1667
21. Sinha Ray S, Okamoto M (2003) Prog Polym Sci 28:1539
22. Sadhu S, Bhowmick AK (2004) J Polym Sci Part B: Polym Phys 42:1573
23. Bandyopadhyay A, Bhowmick AK, de Sarkar M (2004) J Appl Polym Sci 93:2579
24. Sengupta R, Bandyopadhyay A, Sabharwal S, Chaki TK, Bhowmick AK (2005) Polymer 46:3343
25. Basiuk EV, Monroy-Pelaez M, Puente-Lee I, Basiuk VA (2004) Nano Lett 4(5):863–6
26. Lu KL, Lago RM, Chen YK, Green MLH, Harris PJF, Tsang SC (1996) Carbon 34:814
27. Menczel JD, Jaffe M, Bessey WE (1997) In: Turi EA (ed) Thermal characterization of polymeric materials. Academic Press, San Diego, p 2026
28. Zou Y, Feng Y, Wang L, Liu X (2004) Carbon 42:271
29. Bhattacharyya AR, Sreekumar TV, Liu T, Kumar S, Ericson LM, Hauge R, Smalley RE (2003) Polymer 44:2373
30. Jain A, Vijayan K (2002) J Mater Sci 37:2623
31. Liu X, Wu Q, Berglund LA (2002) Polymer 43:4967
32. Xu G, Feng Z-C, Popovic Z, Lin J-Y, Vittal JJ (2001) Adv Mater 13:264
33. Li S-N, Li Z-M, Yang M-B, Hu Z-Q, Xu X-B, Huang R (2004) Mat Lett 58:3967
34. Product brochure titled ''DuPont engineering polymers—extrusion applications''. Downloaded from http://www.dupont.com/enggpolymers/europe on 20 August 2003
35. Murayama T (1986) In: Mark HF, Bikales NM, Overberger CG, Menges G (eds) Encyclopedia of polymer science and engineering, vol 5. Wiley-Interscience, New York, p 299